

Supplementary Materials for

Mechanism of the allosteric activation of the ClpP protease machinery by substrates and active-site inhibitors

Jan Felix, Katharina Weinhäupl, Christophe Chipot, François Dehez, Audrey Hessel, Diego F. Gauto, Cecile Morlot, Olga Abian, Irina Gutsche, Adrian Velazquez-Campoy, Paul Schanda*, Hugo Fraga*

*Corresponding author. Email: hfraga@med.up.pt (H.F.); paul.schanda@ibs.fr (P.S.)

Published 4 September 2019, *Sci. Adv.* **5**, eaaw3818 (2019)
DOI: 10.1126/sciadv.aaw3818

This PDF file includes:

- Fig. S1. Biochemical characterization of *Tt*ClpP.
- Fig. S2. Characterization of GFP_{SsrA} degradation by *Tt*ClpXP.
- Fig. S3. Characterization of *Tt*ClpP peptidase activity in the absence and presence of bortezomib.
- Fig. S4. Characterization of FITC-casein degradation by *Tt*ClpP in the absence and presence of bortezomib and/or *Tt*ClpX.
- Fig. S5. Ligand validation by 2mF_o-DF_c, omit, and polder maps.
- Fig. S6. Distance RMSD of the 14 alanine tripeptide ligands with respect to their initial bound state in *Tt*ClpP for three independent, 1- μ s-long MD simulations.
- Fig. S7. Analysis of structural differences between *Tt*ClpP and *Ec*ClpP.
- Table S1. Crystallographic data collection and refinement statistics.
- Reference (65)

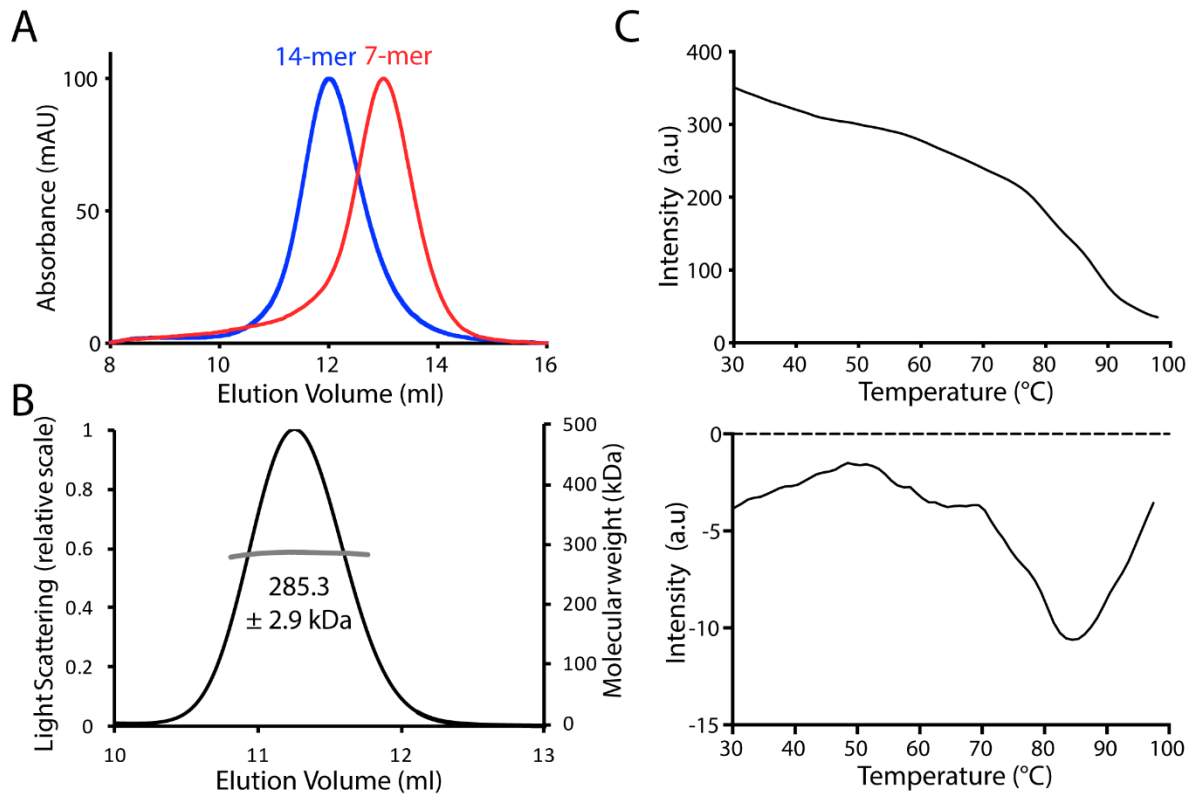


Fig. S1. Biochemical characterization of *TtClpP*. A) Size-exclusion chromatography (SEC) elution profile of *TtClpP*, which elutes as a tetradecamer in a low ionic strength buffer (100 mM NaCl, blue curve). In the presence of 300 mM $(\text{NH}_4)_2\text{SO}_4$ smaller species were observed (red curve) consistent with previously reported heptameric complexes. B) Molecular weight determination of *TtClpP* by MALLS. The light scattering signal (Raleigh ratio, black curve) is plotted as a function of the elution time after SEC. The derived molecular weight (MW, grey curve) represents the average MW across the elution peak. C) The indole group of tryptophan is very sensitive to its environment. The intrinsic fluorescence of *TtClpP*'s single tryptophan (14 per *TtClpP* tetradecamer) was used to monitor *TtClpP* denaturation (upper panel). The melting point of *TtClpP* (concentration: 20 μM) was estimated using the first derivative of the curve (lower panel). (Photo credit: Kyoto University, Primate Research Institute)

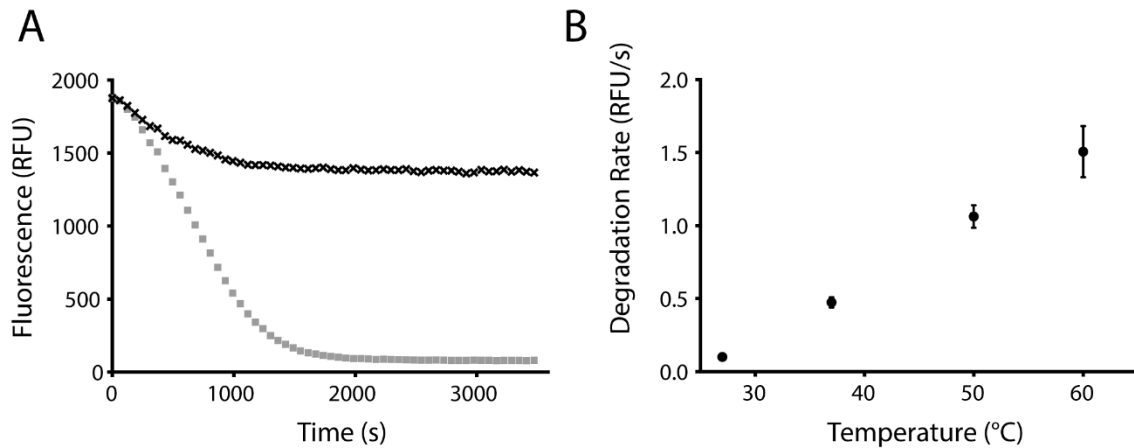


Fig. S2. Characterization of GFPssrA degradation by *TtClpXP*. A) Stable proteins like GFPssrA cannot be degraded by *TtClpP* alone as they cannot access the proteolytic chamber. *TtClpP* (0.1 μM) can, in the presence of *TtClpX* (0.2 μM) and ATP (10 mM), catalyze the degradation of GFPssrA (0.15 μM , grey squares). In the absence of ATP no degradation is observed (black crosses). The small drop in fluorescence observed in the absence of ATP results from temperature equilibrium (assay at 60 °C). B) Initial rates for GFPssrA degradation by *TtClpXP* were plotted as a function of the temperature used. Maximum activity was observed at 60 °C, the maximum incubation temperature allowed in the available fluorimeter. (Photo credit: Kyoto University, Primate Research Institute)

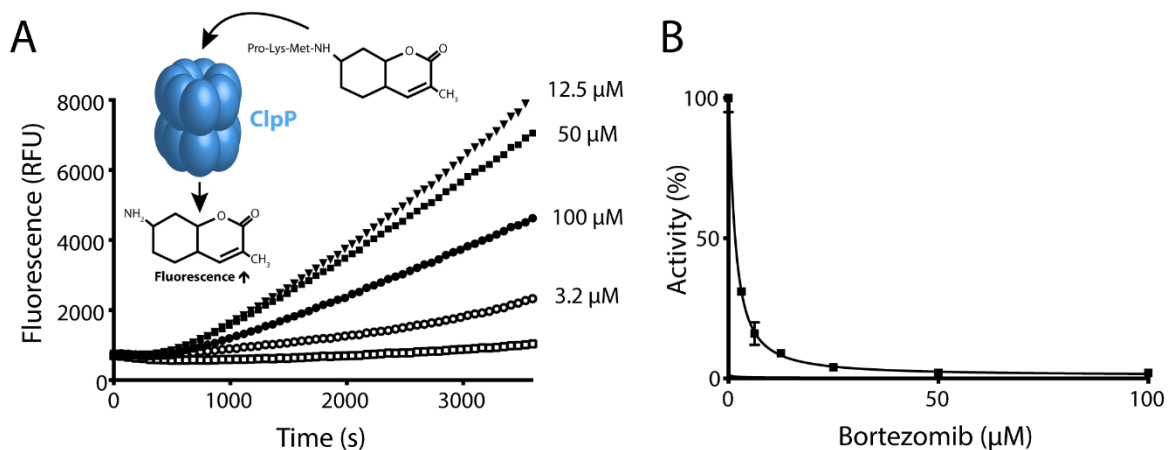


Fig. S3. Characterization of *TtClpP* peptidase activity in the absence and presence of bortezomib. A) *TtClpP* (1 μM) peptidase activity was measured with the substrate PKM-amc (100 μM) in the presence of bortezomib at the indicated concentrations. As the peptide is cleaved, 7-Amino-4-methylcoumarin is released resulting in an increase in the fluorescence measured. B) Bortezomib is an inhibitor of *EcClpP* (0.02 μM) peptidase activity ([PKM-amc]=100 μM) with an IC_{50} of $1.6 \pm 0.1 \mu\text{M}$. (Photo credit: Kyoto University, Primate Research Institute)

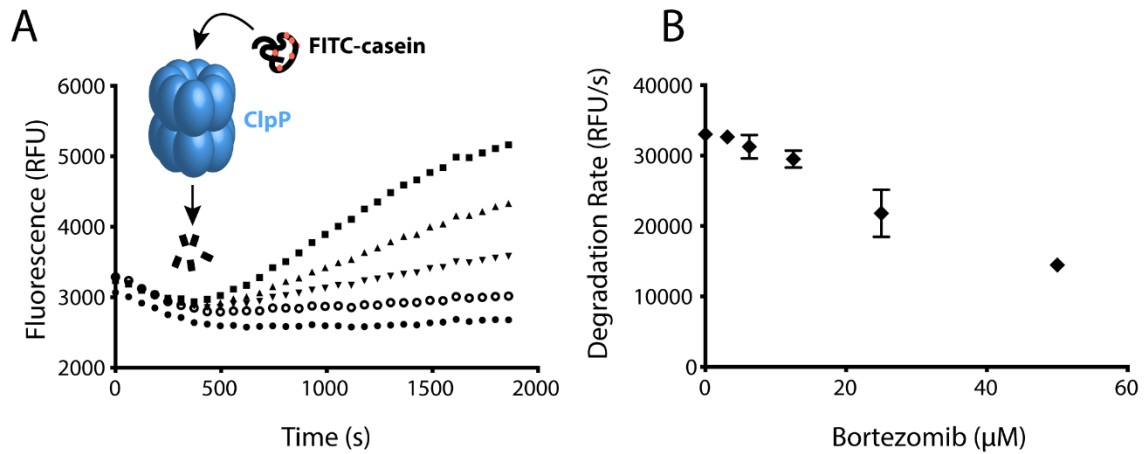


Fig. S4. Characterization of FITC-casein degradation by *TtClpP* in the absence and presence of bortezomib and/or *TtClpX*. A) The degradation of the unfolded protein substrate FITC-casein ($0.15 \mu\text{M}$) by *TtClpP* ($0.1 \mu\text{M}$) was measured in the presence of $100 \mu\text{M}$ bortezomib (squares), $50 \mu\text{M}$ bortezomib (triangle), $25 \mu\text{M}$ bortezomib (inverted triangles), $6.25 \mu\text{M}$ bortezomib (empty circles) and control (filled circles). B) In the presence of *TtClpX* ($0.05 \mu\text{M}$), bortezomib does not activate *TtClpP* ($0.05 \mu\text{M}$) peptidase activity ($[\text{PKM-amc}] = 100 \mu\text{M}$) but instead an inhibition is observed.

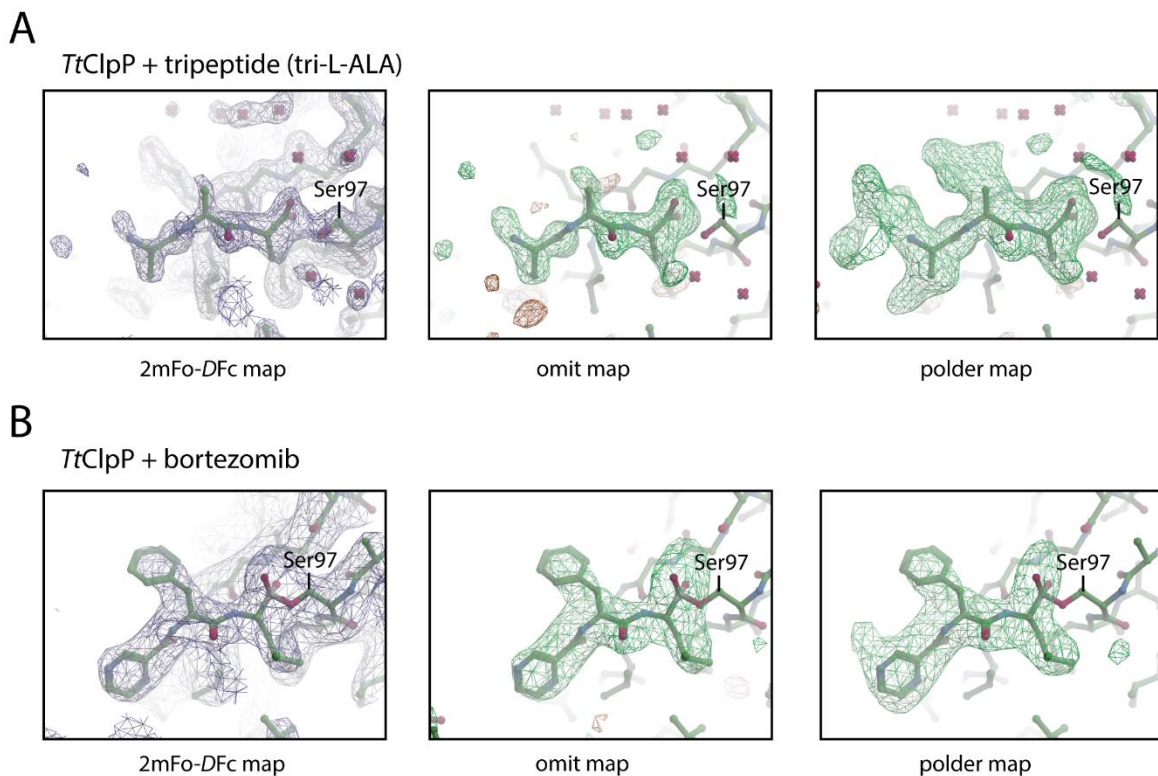


Fig. S5. Ligand validation by $2\text{mF}_o\text{-DF}_c$, omit, and polder maps. $2\text{mF}_o\text{-DF}_c$, omit and polder maps of a tripeptide (A), built as tri-L-ALA, and bortezomib (B) present near Ser97 in the *TtClpP* active site. For the omit and polder maps, $\text{mF}_o\text{-DF}_c$ difference density is contoured at 3σ .

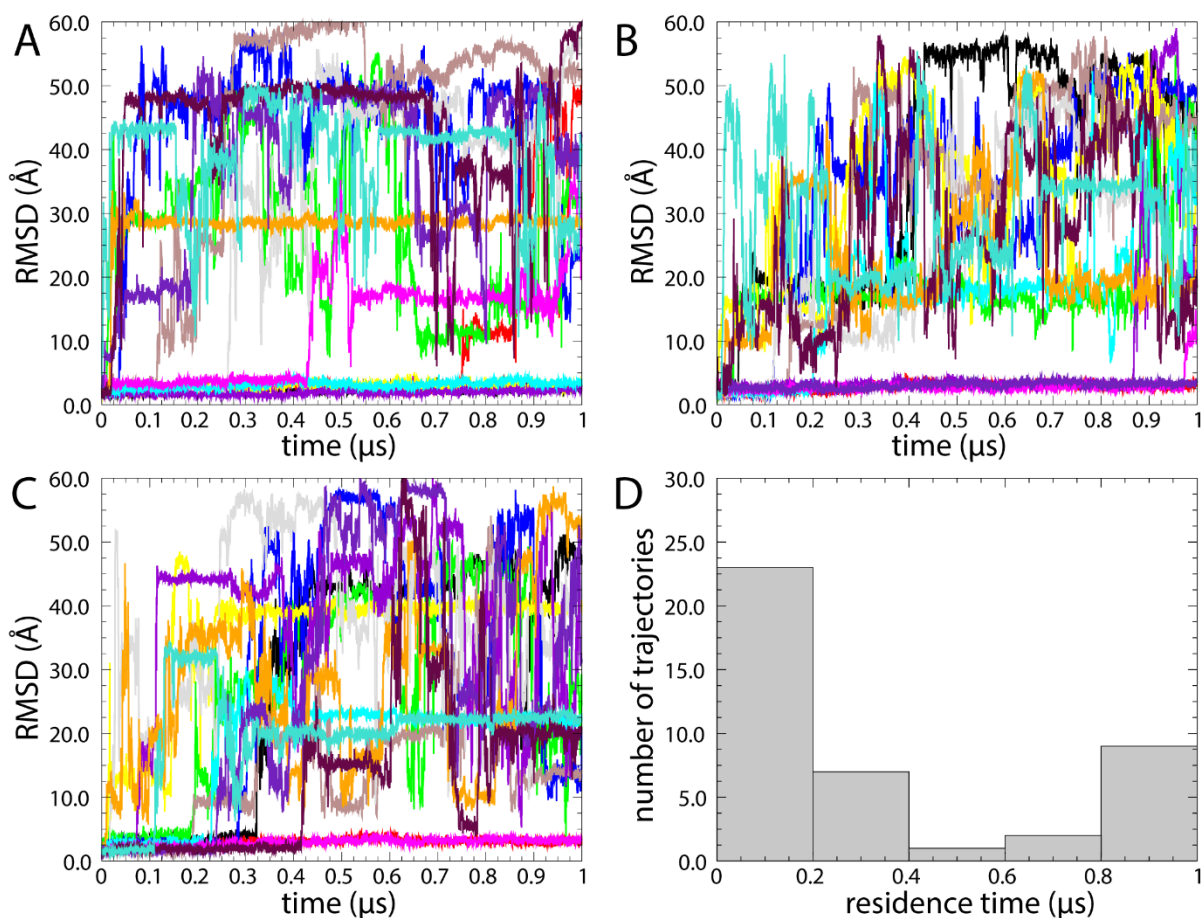


Fig. S6. Distance RMSD of the 14 alanine tripeptide ligands with respect to their initial bound state in *TtClpP* for three independent, 1- μ s-long MD simulations (A-C). Profiles plateauing about 0 reflect a bound state in the initial catalytic site. Distribution of the alanine tripeptide ligands as a function of their residence time in the binding pockets (D). Out of the three simulations \times 14 substrates, nine remain continuously associated to their designated catalytic site (D).

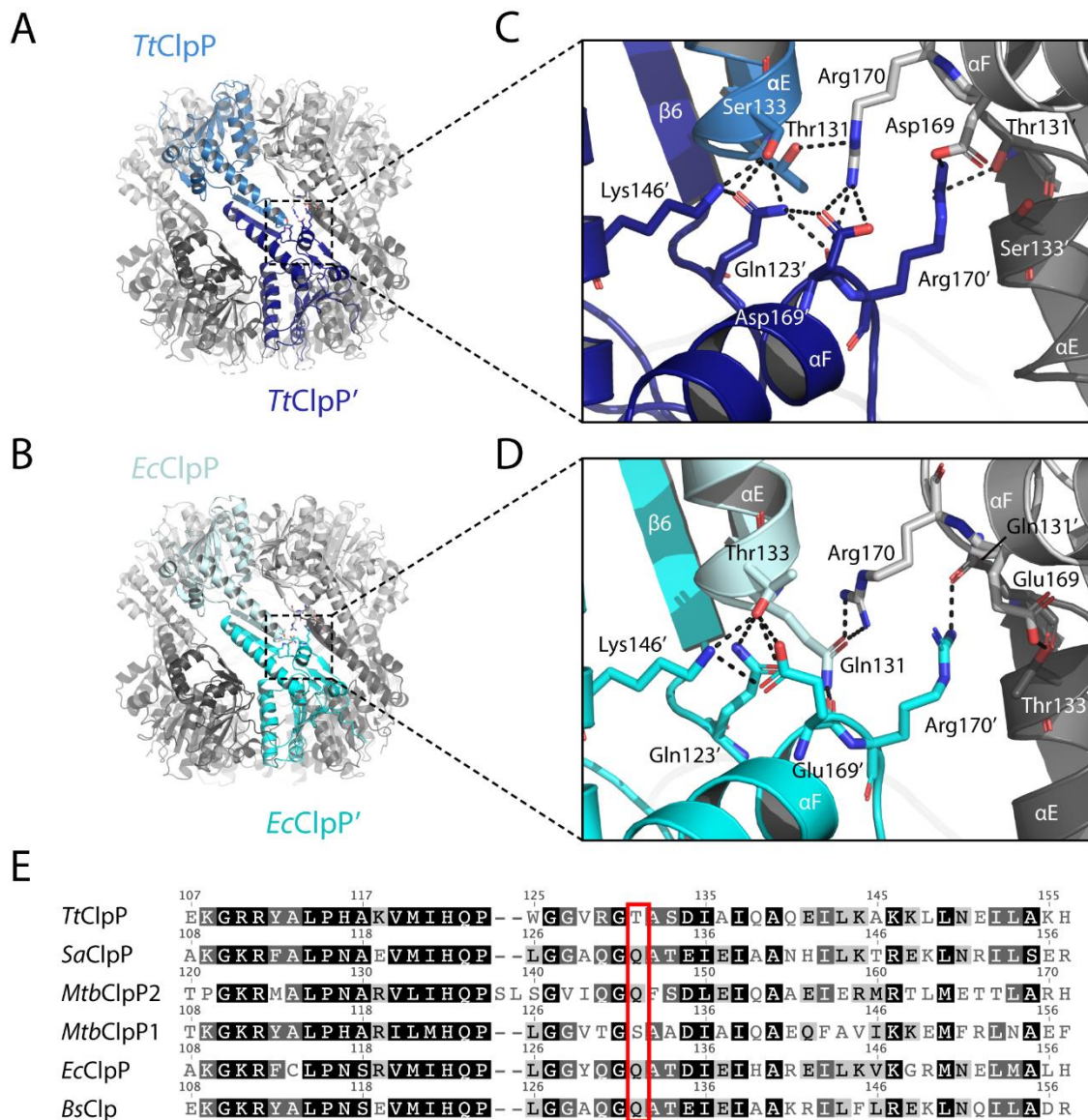


Fig. S7. Analysis of structural differences between *TtClpP* and *EcClpP*. Although the *TtClpP* tetradecameric structure (A) is similar to the previously determined structures of *EcClpP* in the extended conformation (PDB_ID: 1 TYF) (B) differences are found at the tip of the turn that follow helix αE close to β -strand 6 in the handle domain. Residues involved in inter and/or intra-ring contacts are shown as sticks. Note the weaker hydrogen-bonding pattern formed by Thr131 in *TtClpP* (C) versus Gln131 in *EcClpP* (D). Indeed, Gln131 is conserved but replaced by Thr and Ser in *TtClpP* and *MtbClpP1* respectively, as can be seen in the sequence alignment shown in (E).

Table S1. Crystallographic data collection and refinement statistics.

	TtClpP:tripeptide* complex	TtClpP:bortezomib complex
Data collection statistics		
Beamline	ID30A – MASSIF, Grenoble, France	ID23-1 MX, Grenoble, France
Space group	C2	C222 ₁
Cell dimensions		
a, b, c (Å)	105.98, 162.79, 107.95	135.14, 168.74, 166.08
α , β , γ (°)	90, 116.34, 90	90, 90, 90
Resolution (Å)	46.59 -1.95 (2.02 – 1.95)	44.52 – 2.70 (2.796 – 2.7)
Unique reflections	118066 (11696)	52300 (5126)
R_{meas} (%)	7.8 (109.3)	10.2 (265.1)
I/ σ (I)	13.06 (1.56)	16.98 (0.93)
CC(1/2)	99.9 [#] (64.6) [#]	99.9 [#] (64.8) [#]
Completeness (%)	99.25 (98.58)	99.86 (99.57)
Multiplicity	5.3 (5.3)	13.5 (14.3)
Wilson B-factor	35.95	93.62
Refinement		
Resolution (Å)	46.59 – 1.95	46.29 – 2.70
Reflections used in refinement	118029 (11696)	52246 (5104)
Reflections used for R-free	11803 (1169)	5222 (509)
R_{work}/R_{free}	18.58(30.87)/21.09(35.68)	20.26(39.74)/23.45(43.17)
No. atoms	11039	10130
Macromolecules	10289	9913
Ligands	119	217
Solvent	631	-
Average B factor (Å²)	40.88	103.56
Macromolecules	40.14	103.24
Ligands	65.16	117.95
Solvent	48.30	-
Number of TLS groups	14	7
r.m.s. deviations		
bonds (Å)	0.010	0.012
angles (°)	1.24	1.54
Ramachandran favored (%)	98.60	98.44
Ramachandran outliers (%)	0	0
Rotamer outliers (%)	1.33	0.4
Clashscore	5.34	13.65
PDB access code	6HWM	6HWN

Values in parentheses correspond to the highest-resolution shell.

* Due to the unknown nature of the bound peptides, they were built in the electron density as tri-L-Ala

CC(1/2) = percentage of correlation between intensities from random half-datasets. Correlation significant at the 0.1% level is marked by an # (65).